Bioactive Materials 24 (2023) 252–262

Contents lists available at ScienceDirect

Bioactive Materials

journal homepage: www.keaipublishing.com/en/journals/bioactive-materials

A fully biodegradable polydioxanone occluder for ventricle septal defect closure

Zefu Li [a,1], Pengxu Kong [a,1], Xiang Liu [b,c], Shuyi Feng [a], Wenbin Ouyang [a], Shouzheng Wang [a], Xiaopeng Hu [a], Yongquan Xie [a], Fengwen Zhang [a], Yuxin Zhang [d], Rui Gao [c], Weiwei Wang [c,e,*], Xiangbin Pan [a,e,**]

[a] Department of Structural Heart Disease, National Center for Cardiovascular Disease, China & State Key Laboratory of Cardiovascular Disease, Fuwai Hospital, Chinese Academy of Medical Sciences & Peking Union Medical College, National Health Commission Key Laboratory of Cardiovascular Regeneration Medicine, National Clinical Research Center for Cardiovascular Diseases, Beijing, China
[b] Tianjin Key Laboratory of Biomaterial Research, Institute of Biomedical Engineering, Chinese Academy of Medical Science & Peking Union Medical College, Tianjin, China
[c] Department of Polymer Science and Engineering, Key Laboratory of Systems Bioengineering (Ministry of Education), School of Chemical Engineering and Technology, Tianjin University, Tianjin, 300072, China
[d] Research and Development Department, Lepu Medical Technology (Beijing) Co, Ltd, Beijing, 102200, China
[e] Key Laboratory of Innovative Cardiovascular Devices, Chinese Academy of Medical Sciences, China

ARTICLE INFO

Keywords:
Polymer
Congenital heart disease
Ventricle septal defect
Biodegradable occluder
Tissue regeneration

ABSTRACT

Ventricular septal defect (VSD) is one of the commonest congenital heart diseases (CHDs). Current occluders for VSD treatment are mainly made of nitinol, which has the risk of nickel allergy, persistent myocardial abrasion and fatal arrythmia. Herein, a fully biodegradable polydioxanone (PDO) occluder equipped with a shape line and poly-L-lactic acid PLLA membranes is developed for VSD closure without the addition of metal marker. PDO occluder showed great mechanical strength, fatigue resistance, geometry fitness, biocompatibility and degradability. In a rat subcutaneous implantation model, PDO filaments significantly alleviated inflammation response, mitigated fibrosis and promoted endothelialization compared with nitinol. The safety and efficacy of PDO occluder were confirmed in a canine VSD model with 3-year follow-up, demonstrating the biodegradable PDO occluder could not only effectively repair VSD, induce cardiac remodeling but also address the complications associated with metal occluders. Furthermore, a pilot clinical trial with five VSD patients indicated that all the occluders were successfully implanted under the guidance of echocardiography and no adverse events occurred during the 3-month follow-up. Collectively, the fully bioresorbable PDO occluder is safe and effective for clinical VSD closure and holds great promise for the treatment of structural CHDs.

1. Introduction

Ventricular septal defect (VSD) is one of the commonest congenital heart diseases [1,2], leading to pulmonary arterial hypertension and Eisenmenger syndrome with high mortality if untreated [3,4]. Over the past decades, transcatheter VSD closure with occluders has become a preferential therapeutic method due to its advantages such as minimally invasive impact and less complications compared with open-heart surgery [5,6]. Currently, commercially available occluders used for VSD closure are made of nickel titanium (Ni–Ti) alloy due to its shape memory and super-elasticity. However, clinical studies show that metal occluders permanently remaining in the heart may lead to severe complications, such as nickel allergy, myocardial abrasion, valve damage, conduction block, and thromboembolic event, with an overall

Peer review under responsibility of KeAi Communications Co., Ltd.
* Corresponding author. Tianjin Key Laboratory of Biomaterial Research, Institute of Biomedical Engineering, Chinese Academy of Medical Science & Peking Union Medical College, Tianjin, China.
** Corresponding author. Department of structural heart disease, National Center for Cardiovascular Disease, China and Fuwai Hospital, Chinese Academy of Medical Sciences and Peking Union Medical College, Beijing, 100037, No.167 North Lishi Road, Xicheng District, Beijing, China.
E-mail addresses: wwwangtj@163.com, wangww@bme.pumc.edu.cn (W. Wang), panxiangbin@fuwaihospital.org (X. Pan).
[1] These authors are equal contributors.

https://doi.org/10.1016/j.bioactmat.2022.12.018
Received 29 September 2022; Received in revised form 27 November 2022; Accepted 18 December 2022

occurrence rate varying from 0.1% to 8.6% [7–12], which are mainly attributed to long-term release of metal ion, persistent compression on surrounding cardiac tissue, unremitting inflammatory response and delayed process of endothelialization.

Alternatively, biodegradable medical devices provide a promising approach for avoiding the permanent retention of implants [13–17]. Biodegradable materials such as poly (L-lactic acid) (PLLA) and polydioxanone (PDO) with good biocompatibility can fully degrade into carbon dioxide and water, which has been approved by FDA for clinical application in surgical sutures and intravascular stents since 1980s. Occluders made of biodegradable polymers can provide temporary occlusion and induce in situ tissue regeneration with a great hope of solving the problems associated with traditional metal occluders. Clinical trials have demonstrated the feasibility and safety of the PLLA and collagen occluders in atrial septal defect (ASD) closure [18,19]. However, current biodegradable occluders reserve the metal scaffold to provide mechanical support and to enhance the X-ray visibility, which cannot be fully degraded and still confront the risks mentioned above [20,21]. Furthermore, none of the biodegradable occluders have been designed for VSD closure so far. VSD possesses more complicated anatomical structure (e.g., closer to the atrioventricular valve and conduction pathway) and bears greater hemodynamic impact compared with ASD, which demands a higher level for morphological design, mechanical properties and pro-endothelialization of biodegradable occluders. Thus, the closure of VSD using fully biodegradable occluder remains a substantial clinical challenge.

Herein, to address the issues caused by nitinol occluders remaining in the heart, we developed a fully bioabsorbable PDO occluder for transcatheter VSD closure (Fig. 1). PDO occluder with a double-disc shape is composed of a framework and occlude membranes. Our results demonstrated that PDO exhibited excellent mechanical properties, geometry fitness, biocompatibility and degradability. Subcutaneous implants demonstrate that PDO fibers could significantly alleviate inflammation, recruit pro-reparative M2 macrophages, mitigate fibrosis and promote endothelialization compared with nitinol. Successful transthoracic VSD closure using the PDO occluder was performed in canines under echo-Doppler guidance. The 3 years follow up data indicates that the PDO occluder enhanced cardiac tissue infiltration with moderate inflammation response. The process of endothelialization was faster than that of degradation, guaranteeing that no residual shunt or displacement occurred. The frequency of accidental arrythmia decreased with the degradation of occluder and no fatal arrythmia was observed. A pilot clinical study in 5 VSD patients resulted in successful implantation of all implants, effective closure of the VSDs, with no adverse events such as residual shunt, valve damage and fatal arrythmia during the 3-month follow-up. Altogether, PDO occluder displays superior safety and effectiveness over nitinol occluder for VSD treatment in our bench-to-bedside translational studies, holding great promise for further large-scale clinical trials.

2. Materials

2.1. Fabrication of the occluder

The bioabsorbable occluder was composed of a PDO skeleton and PLLA occlude membranes. The PDO monofilaments were made by melt spinning. PDO granules (Shanghai Shape Memory Alloy Co. Ltd) with a number-average molecular weight of 180 kDa were heated to 160 °C. After melting, PDO was squeezed out from a spinning machine and cooled in water bath to form monofilaments with a diameter of 0.15 mm. A PDO monofilament with a length of 3 m was braided into a net tube and put into a designed mold. The PDO was heated to 100 °C for 60 min and cooled down to room temperature to form the double-disc shape. After that, two occlude membranes, which were made of PLLA by melt spinning with a thickness of 0.1 mm, were cut into the matched size by laser, and were fixed by PDO monofilament on the discs and the waist of the occluder.

2.2. Physical and chemical characterization of PDO

The structure of the polymer was determined by ^{1}H nuclear magnetic resonance (^{1}H NMR) spectra using AVANCE IIITM HD 400 MHz (NanoBAY, Switzerland). Samples were solved in hexafluoroisopropanol using tetramethyl silane (TMS) as the internal reference.

The crystallization property of the polymer was measured by X-ray diffraction (XRD) (Rigaku Ultima IV, Japan) using Cu Kα radiation (λ = 1.5418) at 40 kV and 40 mA in the range of 5–90° with a rate of 5°/min.

The molecular weight and polydispersity of the polymer were analyzed by gel permeation chromatography (GPC) at 30 °C with PL GPC 50 (Polymer Laboratories, UK). Hexafluoroisopropanol was used as

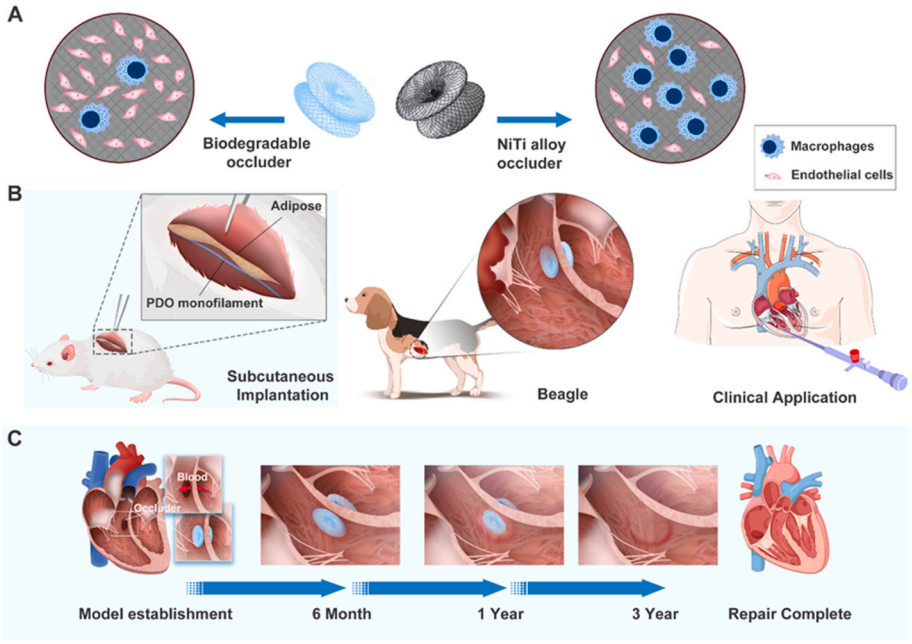

Fig. 1. Schematic diagram of the PDO occluder for VSD closure. (A) Biodegradable and biocompatible PDO occluder could significantly alleviate inflammation and promote endothelialization compared with NiTi alloy occluder. **(B)** The safety and effectiveness of PDO occluder was verified in a rat subcutaneous implantation model, a canine VSD model, and a pilot clinical application for 5 VSD patients. **(C)** 3-year follow-up of canine VSD model demonstrated the process of the occluder-induced cardiac repair.

eluent at a flow rate of 1.0 mL/min. The sample concentration was 1 mg/mL.

The thermal properties of the polymer were determined by differential scanning calorimetry (DSC) (DSC Q2000, USA). Samples of PDO were heated to 160 °C and maintained for 5 min to remove thermal history, then were cooled to −80 °C at a rate of 10 °C/min, and were reheated to 160 °C at the same rate.

The thermal stability of the polymer was measured by thermogravimetric analysis (TGA) (Rigaku TG-DTA8122, Japan). The weight loss was measured in a nitrogen environment with a temperature range from 30 to 450 °C at a rate of 5 °C/min.

The mechanical properties of PDO monofilaments were assessed by an electronic universal testing machine (Instron, USA). The length of PDO sample was 3 cm and the diameter was 0.15 mm. The tensile velocity was 15 mm/min.

2.3. Fatigue fracture analysis of PDO occluder sample

The multi sample fatigue testing system (3330-MSF Series II, BAHENS, Shanghai, China) was calibrated as the following settings: loading: ±3000 N; shifting: ±12.5 mm; loading accuracy: ±0.5%; shifting accuracy: ±0.5%. The test sample occluders were fixed into the center of cartridge stationary ring with a 13 mm aperture and 8 mm in thickness. Properly deployed occluders were immersed in the thermostatic waterbath (37 °C) full of phosphate buffer.

Serving as the inflow end-surface, the left ventricular disk of the occluder was forced to reach a unilateral displacement of 2.55 mm after the adjustment of the testing system with a steady frequency of 1.2hz. Stereomicroscope (ZOOM645S, Wence, Shanghai, China) was used to observe fracture or crack of the framework after 9.5 million times of circulation cycles. Fracture, crack, deformation, structural defect and other forms of damage were recorded accordingly.

2.4. Shape recovery percentage of PDO occluder

PDO occluder was loaded into a 10F catheter and then was pushed forward via manipulating a push shaft to simulate the delivery, deployment and shaping process in vitro. The shaping line assisted in reshaping the disc after the occluder was completely released from the 10F delivery sheath. The diameter of the left disc and right disc of the occluder in the original shape, delivery, releasement and shaping was measured and compared in each operating step. The shape recovery percentage of PDO occluder = Diameter of the disc (delivery, releasement and shaping)/diameter of the disc in original shape.

2.5. Toxicity and hemolysis

Cell counting kit-8 was used to evaluate the cell cytotoxic of the PDO. PDO samples were sterilized by 75% ethanol, rinsed by PBS and were immersed in cell culture medium for 24 h to obtain extract liquid. The L929 cells were seeded at a density of 5000 cells/well in 96-cell plates and cultured at 37 °C in 5% CO_2 atmosphere for 24 h, supplemented with 90% Dulbecco's Modified Eagle's Medium (DMEM), 10% fetal bovine serum, 1% penicillin and streptomycin. After that, the cell cultural medium was replaced by the extracted liquid and the cells were cultured for another 1, 3 and 5 days. The extracted liquid was replaced by new medium with a ratio of DMEM and CCK-8 kit (Dojindo, CK04) of 9:1 and cells were cultured for another 1 h. Cell culture medium was used as positive control. The absorbance was measured at 450 nm.

Calcein/PI cell viability/cytotoxicity assay was used to visualize the morphology and cell viability. The L929 cells were seeded in 24-cell plates at a density of $2*10^4$ cells/well and cultured at 37 °C in 5% CO_2 atmosphere for 24 h. Then the cells were cultured in extracted liquid for another 3 and 5 days. After incubation with Calcein/PI mixture solution for another 30 min, the cell viability/cytotoxicity was evaluated using fluorescence microscope (Leica microsystems, Germany). The live cells were stained with green (Calcein) and the dead cells were stained with red (PI).

Fresh rabbit whole blood was diluted in saline at a volume ratio of 4:5. The samples of PDO were sterilized and immersed in 10 mL saline at a ratio of 1.25 cm^2/10 mL at 37 °C for 30 min. Then 0.2 mL diluted blood was added and cultivated at 37 °C for 1 h. After centrifugation at 3000*g* for 5 min, the supernatant of samples was collected for absorbance measurement at 545 nm by an enzyme standard instrument. Sterilized deionized water and saline were used as positive and negative control. Hemolysis rate was calculated as follows: Hemolysis rate (%) = $(A_s\text{-}A_n)/(A_p\text{-}A_n) \times 100\%$, where A_s, A_p and A_n represent the absorbance of samples, positive control and negative control.

2.6. Animal model

Beagle dogs weighting from 8.10 to 10.40 kg were used for implantation of the PDO occluders. The animals were purchased and supported from the Sichuan Chengdu Beagle Breeding Base (Sichuan, China) and Center for Experimental Animals of Fuwai Hospital (Beijing, China). Provided by Vital River Laboratory Animal Technology (Beijing, China), Sprague-Dawley rats (male, 200–220 g, 6 weeks) were used to investigate the biocompatibility of degrading PDO fibers. The research protocol and animal welfares involved in this study were approved by the department of the Ethics Committee on Animal Study of Fuwai Hospital (FW-2022-0014) and Ren Chonghe Hospital (ACU-2014shxz-0011).

2.7. Subcutaneous implantation of PDO in rats

Eighteen male SD rats were used for subcutaneous implant studies. Animals were anesthetized using isoflurane before the surgery. The back hair was shaved, and animals were placed over a heating pad for the duration of the surgery. The dorsal subcutaneous space was accessed by a 1–2 cm skin incision in the center of the animal's back for implantation. Blunt dissection was performed from the incision toward the animal shoulder blades. Both PDO monofilament (15 mm in length, 0.15 mm in withth) and nitinol wire (15 mm in length, 0.15 mm in width, Shanghai Shape Memory Alloy Co. Ltd) were placed on separate subcutaneous tissue in each rat (n = 3 for each time point). SD rats with skin incision and seaming were set as sham control group (n = 3 for each time point). At 1week, 1 month and 3 months after implantation, subcutaneous regions of interest were harvested and fixed in 4% formalin for 3 days for further histological analyses.

2.8. Transcatheter VSD occlusion in canine model

Eighteen beagle dogs (male, 8–10 kg) were implanted with the PDO occluder through small incision of right chest. Specifically, thoracotomy surgery was performed through the right chest 3–4 intercostal incision after anesthesia. The right ventricular free wall was exposed to avoid coronary artery branches, and a purse string suture was performed near the right bottom with 4-0 proline suture. Next, a blunt needle was inserted into the right ventricular free wall through the 6F artery sheath at the center of previous purse-string suture. The acupuncture proceeded and completed when the needle tip penetrated periventricular septum under the guidance of transthoracic echocardiography (TTE). The ventricular septal defect was dilated using a 6 mm diameter balloon dilatation catheter to create VSD models. The diameter of selected occluders with a 11 mm diameter of disc and 6 mm height of the waist matched the size of the VSDs which were created in the dogs. 10F sheath was used to deliver the occlusion system. The PDO occluder was connected to the clamp of the delivery system and loaded into the sheath, and then advanced into the left ventricle under ultrasound guidance. The left-side disc was expanded in the left ventricular cavity. After ensuring that the left-side disc had clung to the ventricular septum, the sheath was withdrawn to deploy the right-side disc. The shaping line was tightened

to reshape the double-disc formation. Echocardiography was utilized to confirm the location of the occluder and assess residual shunt. After checking that both discs were well unfolded and positioned, the occluder was released by releasing the rostral forceps. Ampicillin (1 g) was administered intravenously after implantation and all beagles received aspirin (5 mg/kg/d) postoperatively for 3 days. General characteristics and laboratory test results were recorded.

Animals were followed up at 1, 3, 6, 12, 24 and 36 months (n = 3 for each time point). We performed TTE, electrocardiogram and hematological tests at each point. The diameters of the left and right discs of the occluder were measured by echocardiography at different follow-up points to evaluate the degradation. Besides, we carried out gross anatomical examination, histologic evaluation and scanning electron microscope (SEM) observations after sacrificing three experimental beagles at each time point.

2.9. Histology, immunohistochemical and immunofluorescence staining

The fixed tissues were dehydrated and further embedded. The cross sections of subcutaneous implantation and intracardiac occluder were stained with hematoxylin and eosin (H&E), Masson's trichrome. The images were obtained through a whole-slide imaging system (Pannoramic, 3Dhistech, Hungary). Collagen volume fractions (CVF) and inflammation area fraction of different subcutaneous embedding groups were quantitatively measured by ImageJ (version 2.1.0, National Institutes of Health, USA).

Subcutaneous implantation was assessed using immunohistochemical and immunofluorescence staining of markers (supplementary Materials), including CD68, CD206, iNOS (inducible nitric oxide synthase) and CD31. Images were obtained through a laser confocal microscope (SP8, Leica) and the whole-slide imaging system (Pannoramic, 3Dhistech, Hungary).

2.10. Western blot assays

Tissues collected from subcutaneous implant sites were lysed using a commercial sample buffer containing a protease and phosphatase inhibitor cocktail (MagNA Lyser Green Beads, Roche, Switzerland). The protein concentration was determined using a BCA Protein Assay Kit (P0012, Beyotime, China); the total protein was separated using NuPAGE 4–12% Bis–Tris Gel (NP0322BOX, Invitrogen, USA) and then transferred to 0.45 μm polyvinylidene fluoride (PVDF) membranes (IPVH00010, Merck Millipore, USA). Non-specific binding was blocked with QuickBlock™ blocking buffer (P0252, Beyotime, China) at room temperature for 15 min. The membrane was then incubated with corresponding diluted primary antibodies [mouse anti-CD206 (1:1000; 60143-1-Ig, Proteintech); rabbit anti-CD31 (1:1000; ab222783 Abcam); rabbit anti-CD68 (1:1000; ab125212, Abcam); rabbit anti-iNOS (1:1000; 18985-1-Ag, Proteintech)] overnight at 4 °C. GAPDH was used as an internal control to normalize protein bands. After washing with TBST for 3 cycles with 10 min each, the membranes were incubated with appropriate secondary antibodies for 1 h at room temperature. Specific antigen–antibody binding bands were visualized using the ultra-high sensitivity ECL chemiluminescence kit (P0018AS, Beyotime, China). Representative protein binding bands were acquired by automatic chemiluminescence image analysis system (4600, Tanon, Shanghai).

2.11. Pilot clinical study

The pilot clinical study of the biodegradable PDO occluder was performed in Fuwai Hospital of Chinese Academy of Medical Sciences, Beijing. All the procedures were approved by the ethics committees of Fuwai Hospital. Written informed consent was obtained from all patients/guardians.

Patients with perimembranous VSD were screened for this study. PDO occluders with diameters varying from 5 to 7 mm were implanted through a transcatheter approach under the TTE guidance [22]. All patients underwent electrocardiography and laboratory tests at discharge, 30 days and 3 months.

2.12. Statistical analysis

Statistical analysis was performed with GraphPad Prism version 8.3.0. Continuous data are presented as mean ± standard deviation (SD). Student t-test was applied for comparisons between two groups, and one-way ANOVA followed by Bonferroni post hoc test was used to analyze differences between multiple groups. Statistical significance is denoted by *$p < 0.05$, **$p < 0.01$, and ***$p < 0.001$.

3. Results

3.1. Design of the fully bioabsorbable occluder

As shown in Fig. 2A, the fully bioabsorbable double-disk occluder is composed of the framework and the occlude membranes. First, granules of PDO were melt and extruded to form monofilaments. After that, PDO monofilaments were cut into segments with length of 2–5 m for knitting occluders with waist diameters ranging from 5 to 14 mm. The monofilaments were braided into net tubes and heat-set in a mold to form double-disc shape. The shape memory and elasticity of PDO materials are inferior to those of Ni–Ti alloy, which could adversely affect the morphology of the occluder after releasing from the catheter. To strengthen the geometry fitness of PDO skeleton, a shape line made of PDO monofilament was knitted on the left disc, which could be tightened to compress and shape the discs after the occluder was deployed from the catheter (Fig. 2B and C). The diameter of the waist was 5 mm smaller to that of the discs to minimize the compression on surrounding cardiac tissue caused by the occluder (Fig. 2A). PLLA occlude membranes were wrapped in the double discs to further prevent residual shunt. The delivery system was made up of a stainless-steel spring tube with a clamp on the tip (Fig. 2B). A knot on the right disc was designed for clamping during the delivery of the occluder (Fig. 2B). Notably, we removed all metal markers, which endowed the PDO occluder with full biodegradability.

3.2. Physical and chemical characteristics of PDO

The biocompatibility, degradation rate and mechanical properties of biomaterials depends on physicochemical property such as crystallinity, molecular weight, molecular weight distribution. Therefore, physical and chemical properties of the PDO were characterized. The structure of PDO polymer was determined by ^{1}H NMR (Fig. 2D). The signal of methylene group of PDO at 3.51 ppm, 3.36 ppm and 2.96 ppm, respectively. The molecular weight distribution of the PDO was determined by GPC. As shown in Fig. 2G, the retention time was 11.6 min. The number average molecular weight Mn, weight average molecular weight Mw, polydispersity [Mw/Mn] were 61 kDa, 103 kDa and 1.69, respectively.

The crystalline state of PDO was analyzed by XRD, which showed a characteristic diffraction peak at 22.4° (Fig. 2E). The thermal stability of PDO was analyzed by TGA. The TGA curve showed a decomposition range from 198 to 290 °C, with the maximum rate temperature (Tmax) at 276 °C (Fig. 2F). A typical DSC curve shows that glass transition temperature, crystallization temperature and melting point occurred at −7.15 °C, 39.09 °C, and 109.54 °C (Fig. 2H), respectively. The endothermic melting enthalpy (ΔH_m) was calculated to be 67.77 J/g. The degrees of crystallinity $\chi c = \Delta H_m/\Delta H_{m0} = 48.0\%$, where the ΔH_{m0} represents the melting therapy of fully crystalline PDO from the heating trace and equals to 141.2 J/g [23,24]. These data demonstrate the thermal-stability of PDO and the suitability for hot-working treatment.

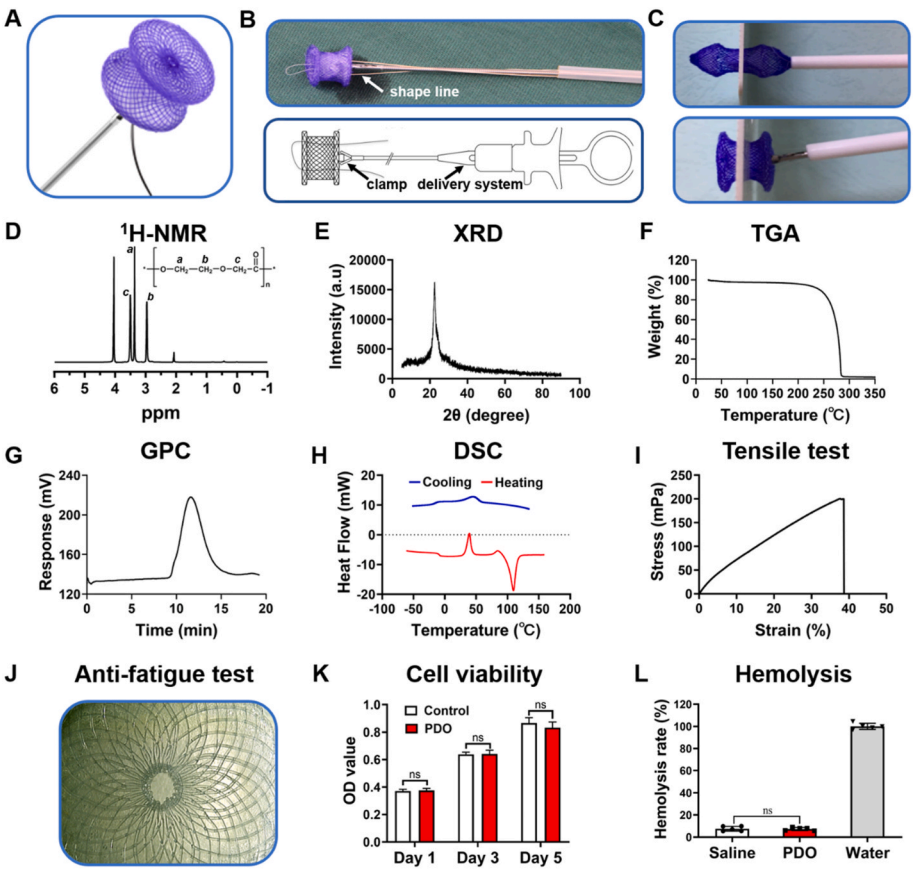

Fig. 2. Design, characteristics, biocompatibility of PDO occluder. (A, B) Design of PDO occluder and delivery system. **(C)** Morphology of PDO occluder released from the sheath before (above) and after (below) the shape line was tightened. **(D)** ^{1}H NMR; **(E)** XRD; **(F)** TGA; **(G)** GPC; **(H)** DSC of PDO. **(I)** Tensile test of PDO monofilament. **(J)** Microscopic image of right disc of PDO occluder after anti-fatigue test. **(K)** Cell viability determined by CCK-8 assay. **(L)** Hemolysis test of PDO monofilament.

3.3. Anti-fatigue performance and shape recovery of PDO occluder

VSD occluder should bear blood flow impact of >100 mm Hg and suffer ~100 thousand cycles of contraction and relaxation in a day. Therefore, the occluder was expected to preserve steady structure under highly intensive impact. The representative of tensile test for PDO filament indicates that the tensile strength and elongation at break was 200.17 mPa and 38.6% (Fig. 2I).

After 9.5 million cycles of fatigue test (equivalent to 3 months of heartbeat cycle) with loading of 300sl0 N and shifting of 12.5 mm, the structure of PDO occluder was intact. No fracture, rupture or delamination of occluder were observed in microscopic examination (Fig. 2J and S1), suggesting that the PDO occluder could adapt to the blood pressure in the ventricle without deformation or fracture.

The deformation of the occluder after one time of in-and-out of the sheath was recorded. The diameter of the right disk and left disc were 96% and 94% of the original diameter respectively (Fig. S2).

3.4. In vitro biocompatibility of PDO

CCK-8 and Live/Dead staining were performed to assess the biocompatibility of PDO. As shown in Fig. 2K, the cell viability was comparable between control and PDO group at 1, 3 and 5 days. No obvious difference was observed in the amount and morphology of live cells between the two groups (Fig. S3). Hemolysis test showed that only less than 1% hemolysis was observed in the PDO group (Fig. 2L). These results indicated that PDO was nontoxic and biocompatible.

3.5. Less inflammation and favorable endothelialization of PDO in vivo

To further evaluate the biocompatibility in vivo, PDO fibers and nitinol wires as a positive control were implanted subcutaneously (Fig. 3A). Masson's trichrome staining showed that collagen was distributed in a significantly higher density in the nitinol group compared with PDO group at 1 week, 1 month and 3 months (Fig. 3B and C), indicating that foreign body response and fibrotic encapsulation caused by PDO were milder than that caused by nitinol. H&E staining further demonstrated the inflammation area characterized by the infiltration of neutrophils and macrophages in the nitinol group was larger than that in PDO and sham group at 1 week and 1 month (Fig. 3D and E). The inflammatory response caused by PDO was similar to the sham group after 1 month. These data indicated that PDO could induce a less intensity and shorter duration of inflammatory response, showing greater biocompatibility compared with nitinol.

Macrophages play a central role in foreign body response and are closely related to duration of inflammation. Macrophage can be polarized into two classically described group: pro-inflammatory M1 (iNOS^{+}) or pro-reparative M2 (CD206^{+}) phenotype, which may be influenced by physical and chemical properties of materials. To further investigate the inflammatory response, immunofluorescence was utilized to elucidate the phenotype of macrophage. As shown Fig. 4A, the number of macrophages (CD68^{+}) recruited in the PDO group was significantly lower than that in nitinol group. In addition, more M2 type macrophages were polarized in the PDO group, indicating the reparative process induced by PDO (Fig. 4A). The results of immunofluorescence were further validated by immunohistochemistry (Fig. S4) and western blot (Fig. 4B). The expression of CD68 and iNOS were significantly up-regulated in the nitinol group whereas the CD206 was up-regulated in PDO group. These results showed that the PDO facilitated a pro-reparative response in vivo.

Biodegradable materials are conducive to cell adhesion and infiltration, which could promote progress of endothelialization. To evaluate the endothelial cells adhesion, we assessed the expression level of CD31, a marker of endothelial cells by immunofluorescence and

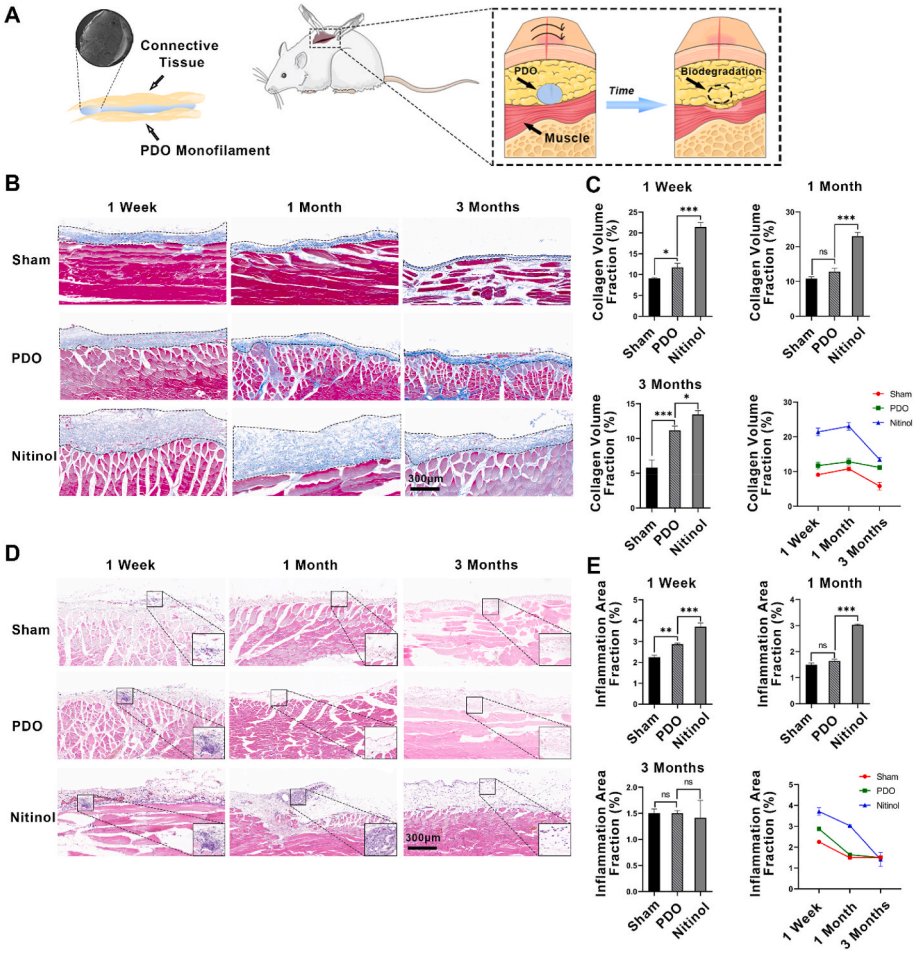

Fig. 3. PDO monofilament causes less fibrosis and inflammation in a rat subcutaneous implantation model. (A) Schematic presentation for subcutaneous implantation of PDO monofilament and nitinol wire. **(B)** Masson staining of tissues of sham, PDO and nitinol group at 1 week, 1 and 3 months, respectively. **(C)** Statistical analysis of collagen volume fraction of control, PDO and nitinol groups (n = 3). **(D)** Representative images of H&E staining of control, PDO and nitinol groups. **(E)** Statistical analysis of inflammation area fraction of control, PDO and nitinol groups (n = 3). *P < 0.05. **P < 0.01. ***P < 0.001. ns, not significant. The black dotted lines indicated the interface between implants and tissue.

immunohistochemical staining. As shown in Fig. 4C and Fig. S4, compared to nitinol, PDO significantly increased the intensity of CD31-positive endothelial cells at 1 month, indicating a favorable endothelialization progress. Western blot also showed that the expression level of CD31 was also significantly up-regulated in the PDO group (Fig. 4D), indicating that PDO favored the endotheliocyte adhesion and infiltration, which could promote the progress of endothelialization in vivo.

3.6. Implantation of occluders in a canine VSD model with 3-year follow-ups

For clinical translation, we further evaluated the safety and effectiveness of PDO occluder in a canine VSD model. VSD was created by perforating the ventricular septum and balloon dilatation. The diameters of VSD varied from 4 mm to 5 mm. Transcatheter implantation of occluders was performed under the guidance of TTE. The PDO occluders were clearly visible under the TTE guidance. After being adjusted to an appropriate position, the occluder was released from the delivery system. The shape line of the occluder was pulled to compress the left disc close to the ventricular septum and re-shaped the double discs. All of 18 occluders were successfully implanted on the first attempt. All animals survived in good physical condition after the procedures. No evidence of hematoma, pericardial effusion, valve damage, limb ischemia, dyspnea or infection occurred during the procedures.

At 1, 3, 6, 12, 24 and 36 months, 3 dogs were sacrificed to evaluate the efficacy of the biodegradable PDO occluders at each time point. In the gross examination, occluders were well positioned in the ventricular septum without displacement (Fig. 5A). No thrombus was observed on the surface of occluder. During the follow-up, the residual area of PDO occluders gradually decreased, while the endothelium gradually covered the discs (Fig. 5A), suggesting the process of degradation and endothelialization.

H&E staining showed that no severe inflammation, thrombus, or myocardial abrasion occurred in the heart during the follow-up (Fig. 5B). Moderate inflammatory response was observed within 6 months. The residual PDO was clearly observed with a mean diameter of 183 μm from 1 to 6 months, which was gradually degraded and the diameter of PDO fibers decreased to 126 μm at 12 months and mostly degraded at 24 and 36 months. As shown in Fig. 5C, Masson trichrome staining showed that the endothelium grew from the edge of the PDO framework to the center of the occluder with the collagen disposition surrounded the PDO filaments. The surrounding myocardium was intact and no scar formation was observed, indicating that the occluder would not persistently compress or abrase the cardiac tissue (Fig. S5).

As shown in Fig. 5D, the amplitude of the increase in endothelium coverage area from implantation to 12 months (0%–78%) was significantly larger than that of the decrease in PDO residual area (100%–56%), demonstrating that the endothelialization rate was markedly faster than the degradation rate. The PDO did not completely degrade until 24 months while endothelium could cover and encapsulate most PDO filaments at 6 months, suggesting that PDO could maintain the scaffold for endothelial adhesion until the full endothelialization, which guaranteed the stability of the occluder and avoided the residual shunt.

Scanning electron microscope showed that PDO filaments remained at 3 months with endothelium surrounded. The PDO occluder was fully degraded at 36 months with reconstruction of a highly fibrillar microarchitecture, which was similar to the structure of native myocardium (Fig. 5E).

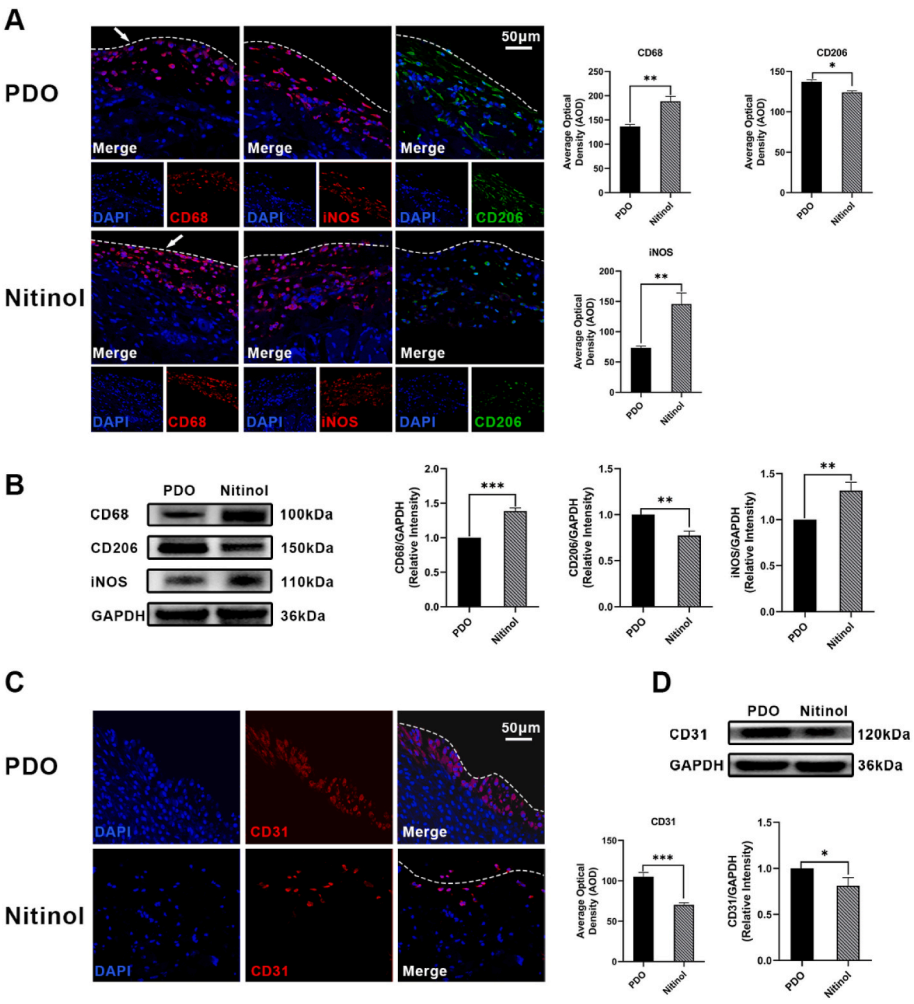

Fig. 4. PDO promotes pro-reparative macrophage polarization and endothelialization. (A) Representative immunofluorescence staining of CD206, CD68, iNOS at 1 month after implantation. Average optical density (AOD) was measured (n = 3). **(B)** Protein expression level of CD68, CD206 and iNOS in tissues determined by western blotting (n = 3). (C) CD31 immunofluorescence staining of tissues at 1 month (n = 3). (D) Protein expression level of CD31 in tissues (n = 3). *P < 0.05. **P < 0.01. ***P < 0.001. ns, not significant. The white dotted lines indicated the interface between implants and tissue.

No fatal arrhythmias were observed by ECG during the follow-up and frequencies of arrhythmias were accidental and transient (Fig. 6A). The total frequencies decreased by time with the degradation of the occluder. TTE showed that the occluder was in good position and degraded gradually at each time point (Fig. 6B). Interestingly, the area of the left disc decreased slightly faster than that of the right disc, which was probably attributed to the higher blood flow impact in the left ventricle (Fig. 6B). No residual shunt was observed surrounding the occluder. (Fig. 6B). Cardiac function and morphology were in the normal range during the follow-up (Fig. 6C–E). No abnormalities were found in both blood tests and hepatic examinations, indicating that PDO occluder was not toxic during long-term follow-up (Fig. 6F–H). No thrombus, infarction or PDO residuals were observed in other organs (liver, spleen, lung, and kidney) in gross and microscopic examination (Fig. S6).

3.7. Pilot clinical trial

To further evaluate the safety and effectiveness of the occluder, we performed transcatheter implantation in 5 patients with perimembranous VSD from April 2020 to July 2020. The median age of patients was 4.6 (ranging from 3 to 5) years and the median defect size was 3.7 (ranging from 3 to 4.5) mm. The occluders were implanted using a hybrid perventricular approach under the TTE guidance (Fig. 7A). All occluders were successfully implanted. No major adverse events including cardiac arrest, aggravation of aortic or tricuspid regurgitation, pericardial effusion, or cardiac tamponade occurred and no patient required blood transfusion. Notably, the PDO occluder was clearly visible under TTE, which avoided the use of X-ray guidance and the iatrogenic damage caused by contrast agent.

During the 3-month follow-up, the effectiveness of occlusion was measured by TTE. As indicated in Fig. 7B, no residual shunt was detected in all patients and no device displacement and thrombosis were observed. Blood routine, liver and kidney function were all in the normal range during the follow-up (Fig. 7C–H). No new-onset arrhythmia was observed.

4. Discussion

Here we developed a novel fully biodegradable PDO occluder. To the best of our knowledge, this is the first fully biodegradable occluder for clinical VSD closure, with great mechanical strength, fatigue resistance, biocompatibility, degradability and pro-endothelialization, which was testified by subcutaneous and intracardiac implantation. The long-term follow-up of large animals demonstrated the safety and efficacy of the PDO occluder, which could effectively close the defect and balance the process of the degradation and tissue regeneration without occurrence of residual shunt or displacement. At last, the pilot first-in-human trial confirmed the feasibility and safety, showing promise for further clinical application.

VSD is the commonest congenital malformations of the heart, accounting for up to 40% of all cardiac anomalies [2]. Transcatheter VSD closure with minimal trauma have been developed over the past decade for defects difficult to access surgically. However, this technique is not

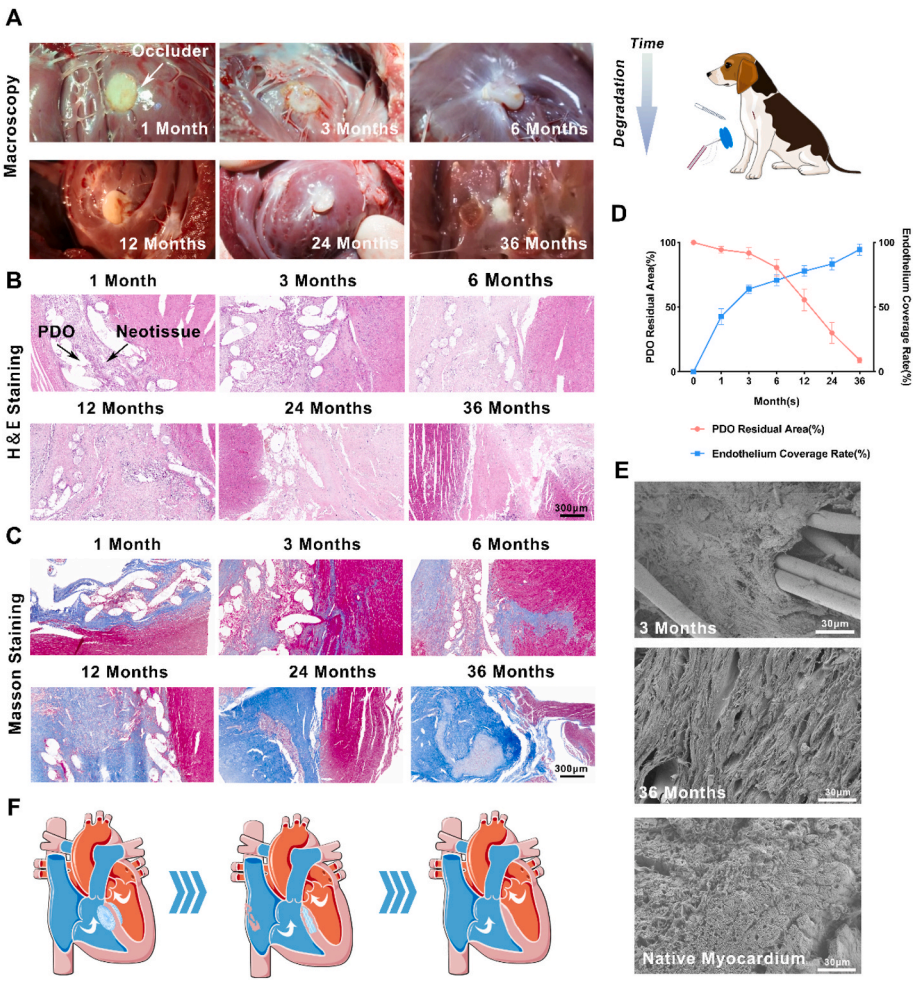

Fig. 5. Safety and efficacy of PDO occluder implanted in a canine VSD model. (A) Macroscopic views of implanted PDO occluders in ventricular septum at 1, 3, 6, 12, 24 and 36 months. **(B)** H&E staining of implanted PDO occluder. **(C)** Masson staining of implanted PDO occluder. **(D)** The PDO residual area and endothelium coverage curves of PDO occluder. **(E)** SEM of implanted occluder harvested at 3 and 36 months and native ventricular septum tissue. **(F)** Illustration of the process of degradation and tissue regeneration.

undertaken in most units and not recommended by guidelines due to the unacceptably high rate of post-procedure heart block associated with currently available devices. The risk does not subside or fall with time, with late-onset heart block being fairly prevalent [25,26], which could be attributed to persistent compression and inflammation response of metal occluders. Currently, multiple types of degradable occluders have been developed for closing congenital heart defects, including the BioSTAR, Carag, BioDisk, which mainly focus on ASD or PFO closure [21,27–29]. Most of them reserve the metal framework, which could assistant in re-shaping the occluder, providing mechanical support and providing X-ray visibility. In this study, to improve the plasticity and geometry fitness between disks and tissue, a shape line was designed, which was knitted on the left disc and could be tightened to enhance the shape retention of the occluder (Fig. 2C). Also, the shape line renders the compact morphology of the occluder after releasing from the sheath without extensive compression on surrounding myocardium, minimizing the risk of cardiac abrasion and arrhythmogenesis. In addition, the crystallinity and molecular weight of the raw PDO materials were modulated to provide proper mechanical strength (tensile strength >200 mPa) and deformation (elongation >30%) to endure blood flow impact and intensive contraction (Fig. 2I). Last, the development of ultrasound-guided procedures enables the design of occluder with fully synthesized polymers without metal markers, and free from the X-ray radiation and the use of metal residuals. Collectively, these technical designs provide physical and biological improvement of the occluders, moving forward for VSD closure with complicated anatomical structure and close relationship with conduction pathway.

Inflammation is closely related to the tissue destruction and new-onset arrythmia [30]. Both operative procedures such as balloon dilatation and occluder contribute to arrythmia. Arrhythmia caused by the balloon dilatation was transient and synchronous with the process of dilatation during the operation, and could recover to normal rhythm quickly after the procedure. However, the arrhythmia caused by the occluder was persistent and even late onset. As shown in Fig. 6A, the occurrence of arrythmia was persistent for more than 6 months. Thus, the new-onset arrhythmia during the follow-up was attributed to occluder. Our results demonstrated that compared with NiTi, PDO exhibited less inflammation response with alleviative inflammatory cell infiltration and higher percentage of M2 type macrophages. (Fig. 4A and B). What's more, the inflammation decreased obviously with the degradation of occluder, which was consistent with the decline of the arrythmia frequency in canine models (Fig. 6A), with the promise of mitigating the risk of late-onset heart block.

While the reasons of the improved inflammation are open at the moment, we try to discuss them briefly. One reason might be a polymer versus a metal with different chemical properties; the other reason might be from a bit cytotoxicity of NiTi. The cytotoxicity of this metal could be alleviated after introducing an appropriate coating, as revealed by Ding team from the orient in their cooperation studies of new occluders of left atrial appendage (LAA) [31]. Their LAA occluder is the first one with nanocoating, exhibits much better cell responses, and has recently been rapidly applied in interventional treatment of heart diseases all over the world. Because our control in studies of VSD occluders is made of NiTi alloy without coating, we cannot distinguish which one of the above two possible reasons is predominant. Nevertheless, our work has developed the first fully biodegradable VSD occluder in clinical

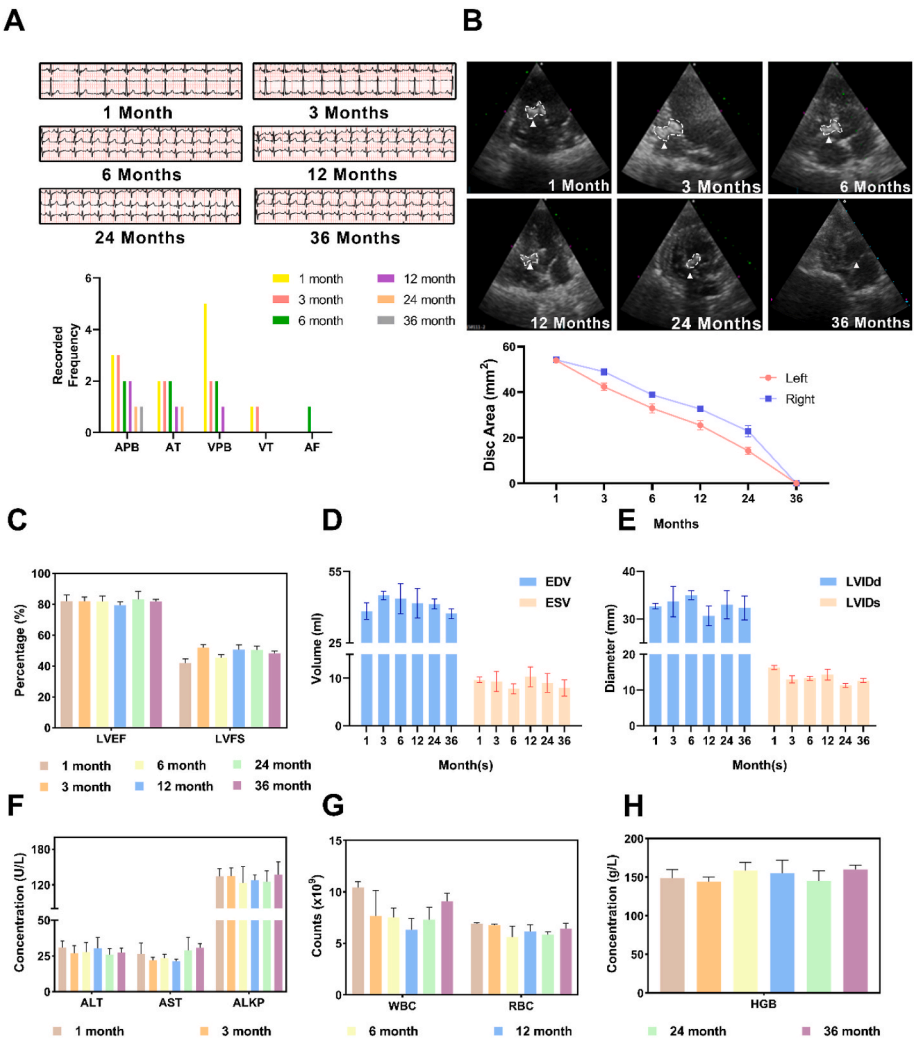

Fig. 6. ECG, ultrasound and blood tests of canine VSD models. (A) Representative images of ECG and frequency of arrhythmia during follow-up. **(B)** TTE images and analysis of left and right disc area. The occluders are outlined with the white dotted line. **(C–E)** Quantification of LVEF, LVFS, LVEDV, LVEDS LVIDd and LVIDs by echocardiography (n = 3). **(F–H)** Quantification of ALT, AST, ALKP, WBC, RBC and HGB (n = 3). APB: atrial premature beat; AT: atrial tachyarrhythmia; VPB: ventricular premature beat; VT: ventricular tachyarrhythmia; AF: atrial fibrillation. LVEF: left ventricular ejection fraction; LVFS: left ventricular fractional shortening; EDV: end-diastolic volume; ESV: end-systolic volume; LVIDd: left ventricular internal dimension in diastolic; LVIDs: left ventricular internal dimension in systole. ALT: alanine transaminase; AST: aspartate transaminase; ALKP: alkaline phosphatase; WBC: white blood cell; RBC: red blood cell; HGB: hemoglobin.

trial and thus has its own value in avoiding the incidence of late complications by using bioresorbable medical device.

The major challenge faced by the development of a biodegradable occluder is to achieve balance between the rate of material degradation and the rate of cardiac tissue generation [12]. Ding et al. have utilized PLLA as a framework and occlude membranes [20]. PLLA is easily available, inexpensive, and has good processing properties. However, the 3-year follow-up of PLLA occluder shows that 3 of 5 ASD patients have residual shunts, which was increased in size over time [18]. We hypothesized that the higher blood impact from the ventricle may accelerate the degradation of PLLA framework and delay the endothelium coverage. Our results revealed that PDO with the presence of ether bonds favored endothelialization, consistent with previous studies [32, 33], thus we chose PDO as a framework and PLLA as occlude membranes. Canine VSD models confirmed that the process of endothelium coverage was faster than that of absorption and the framework could retain its stability in 6 months, which is the time window for endothelium coverage. Intriguingly, the left disc degraded slightly faster than the right disc in the canine model, probably due to the higher blood flow impact from the left ventricle, but both sides remained intact during the 6-month follow-up, indicating that the tissue regeneration and degradation of the occluder were still matched under intensive impact.

The pilot clinical trial including 5 patients in this study displayed promising results. All implantation was successful and no adverse events occurred. The occluders maintained its intact morphology and cling to the ventricular septum without residual shunt at 3 months. No fatal arrythmia was observed during the follow-up. A multicenter, randomized, controlled clinical trial with enrollment of 108 patients and 1-year follow-up has been conducted to validate this novel occluder for VSD closure (NCT03941691). However, our study still has some limitations for future work. First, the mechanisms of alleviative inflammation and fibrosis caused by PDO could be further investigated. Second, although transcatheter access through intercostal space is easier to operate and safer to release occluder, percutaneous intervention through peripheral vessels could minimize the surgical trauma and blood loss during the operation. Moreover, the long sheath used in the percutaneous closure possesses a smaller inner diameter, and a bending and soft head end, while the short sheath used in the transthoracic closure is straight and has a larger inner diameter. Next generation of delivery system through periphery vessels is in development. Third, further evaluation of the patients with long-term follow-up and a larger patient population are needed to fully validate this occluder for VSD closure.

5. Conclusion

In conclusion, PDO occulder with advantages of biocompatibility, mechanical stability, degradation, alleviative inflammation response and pro-endothelialization is a promising candidate for transcatheter VSD closure. We envision that PDO occluder could show the safety and effectiveness in future clinical trials.

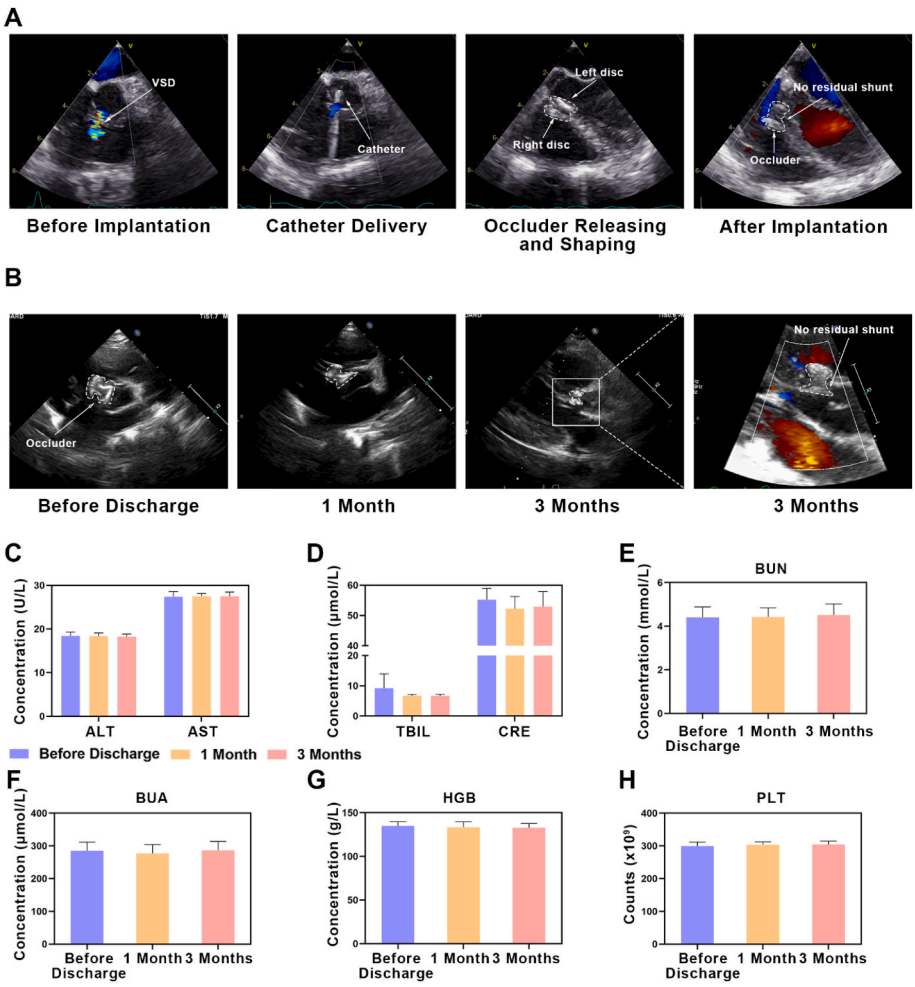

Fig. 7. Clinical application of PDO occluder in VSD patients. (A) Procedures of implantation of PDO occluders under the TTE guidance. **(B)** 3-month follow-up by TTE. TTE: transthoracic echocardiography. **(C–H)** Quantification of ALT, AST, TBIL, CRE, BUN, BUA, HGB and PLT (n = 5). ALT: alanine transaminase; AST: aspartate transaminase; TBIL: total bilirubin; CRE: creatinine; BUN: blood urea nitrogen; BUA: blood uric acid; HBG: hemoglobin; PLT: blood platelet.

CRediT authorship contribution statement

Zefu Li: Conceptualization, Visualization, Visualization, Writing – original draft. **Pengxu Kong:** Conceptualization, Methodology, Writing – original draft. **Xiang Liu:** Methodology, Visualization. **Shuyi Feng:** Visualization. **Wenbin Ouyang:** Investigation. **Shouzheng Wang:** Investigation. **Xiaopeng Hu:** Supervision. **Yongquan Xie:** Supervision. **Fengwen Zhang:** Investigation. **Yuxin Zhang:** Writing – review & editing. **Rui Gao:** Methodology, Investigation. **Weiwei Wang:** Conceptualization, Methodology, Supervision, Writing – original draft, Writing – review & editing. **Xiangbin Pan:** Conceptualization, Supervision, Writing – review & editing.

Declaration of competing interest

All authors declares that there is no conflict of interest

Acknowledgments

Financial support: This work was supported by National Natural Science Foundation of China [81970444], The Fundamental Research Funds for the Central Universities [2019PT350005], Beijing Municipal Science and Technology Project [Z201100005420030], National high level talents special support plan [2020-RSW02], CAMS Innovation Fund for Medical Sciences [2021-I2M-1–065, 2021-I2M-1–058], Sanming Project of Medicine in Shenzhen [SZSM202011013], Natural Science Fund for Distinguished Young Scholars of Tianjin [21JCJQJC00020].

Appendix A. Supplementary data

Supplementary data to this article can be found online at https://doi.org/10.1016/j.bioactmat.2022.12.018.

References

[1] J.I. Hoffman, S. Kaplan, The incidence of congenital heart disease, J. Am. Coll. Cardiol. 39 (12) (2002) 1890–1900.
[2] D.J. Penny, G.W. Vick III, Ventricular septal defect, Lancet 377 (9771) (2011) 1103–1112.
[3] T. van der Bom, A.C. Zomer, A.H. Zwinderman, F.J. Meijboom, B.J. Bouma, B. J. Mulder, The changing epidemiology of congenital heart disease, Nat. Rev. Cardiol. 8 (1) (2011) 50–60.
[4] B.J. Bouma, B.J. Mulder, Changing landscape of congenital heart disease, Circ. Res. 120 (6) (2017) 908–922.
[5] Z.D. Du, Z.M. Hijazi, C.S. Kleinman, N.H. Silverman, K. Larntz, Comparison between transcatheter and surgical closure of secundum atrial septal defect in children and adults: results of a multicenter nonrandomized trial, J. Am. Coll. Cardiol. 39 (11) (2002) 1836–1844.
[6] J.W. Roos-Hesselink, F.J. Meijboom, S.E. Spitaels, R. van Domburg, E.H. van Rijen, E.M. Utens, A.J. Bogers, M.L. Simoons, Excellent survival and low incidence of arrhythmias, stroke and heart failure long-term after surgical ASD closure at young age. A prospective follow-up study of 21-33 years, Eur. Heart J. 24 (2) (2003) 190–197.
[7] A.D. Shah, D.S. Hirsh, J.J. Langberg, User-reported abrasion-related lead failure is more common with durata compared to other implantable cardiac defibrillator leads, Heart Rhythm 12 (12) (2015) 2376–2380.

[8] D. Lakkireddy, D. Thaler, C.R. Ellis, V. Swarup, L. Sondergaard, J. Carroll, M. R. Gold, J. Hermiller, H.C. Diener, B. Schmidt, L. MacDonald, M. Mansour, B. Maini, L. O'Brien, S. Windecker, Amplatzer amulet left atrial appendage occluder versus watchman device for stroke prophylaxis (amulet IDE): a randomized, controlled trial, Circulation 144 (19) (2021) 1543–1552.

[9] U. Krumsdorf, S. Ostermayer, K. Billinger, T. Trepels, E. Zadan, K. Horvath, H. Sievert, Incidence and clinical course of thrombus formation on atrial septal defect and patient foramen ovale closure devices in 1,000 consecutive patients, J. Am. Coll. Cardiol. 43 (2) (2004) 302–309.

[10] S.L. Hill, C.I. Berul, H.T. Patel, J. Rhodes, S.E. Supran, Q.L. Cao, Z.M. Hijazi, Early ECG abnormalities associated with transcatheter closure of atrial septal defects using the Amplatzer septal occluder, J. Intervent. Card Electrophysiol. 4 (3) (2000) 469–474.

[11] Y.J. Kim, S.J. Park, S.Y. Shin, J. Hong, Removed 5-year-old amulet device: triplet of peridevice leakage, poor endothelialization, and device-related thrombus, JACC Cardiovasc. Interv. 14 (21) (2021) 2405–2406.

[12] Y. Wang, G. Li, L. Yang, R. Luo, G. Guo, Development of innovative biomaterials and devices for the treatment of cardiovascular diseases, Adv. Mater. (2022), e2201971.

[13] G. Verreck, I. Chun, Y. Li, R. Kataria, Q. Zhang, J. Rosenblatt, A. Decorte, K. Heymans, J. Adriaensen, M. Bruining, M. Van Remoortere, H. Borghys, T. Meert, J. Peeters, M.E. Brewster, Preparation and physicochemical characterization of biodegradable nerve guides containing the nerve growth agent sabeluzole, Biomaterials 26 (11) (2005) 1307–1315.

[14] H. Tang, Z. Xu, X. Qin, B. Wu, L. Wu, X. Zhao, Y. Li, Chest wall reconstruction in a canine model using polydioxanone mesh, demineralized bone matrix and bone marrow stromal cells, Biomaterials 30 (19) (2009) 3224–3233.

[15] D. Kalfa, A. Bel, A. Chen-Tournoux, A. Della Martina, P. Rochereau, C. Coz, V. Bellamy, M. Bensalah, V. Vanneaux, S. Lecourt, E. Mousseaux, P. Bruneval, J. Larghero, P. Menasché, A polydioxanone electrospun valved patch to replace the right ventricular outflow tract in a growing lamb model, Biomaterials 31 (14) (2010) 4056–4063.

[16] J.H. Lee, J.H. Kim, S.H. Oh, S.J. Kim, Y.S. Hah, B.W. Park, D.R. Kim, G.J. Rho, G. H. Maeng, R.H. Jeon, H.C. Lee, J.R. Kim, G.C. Kim, U.K. Kim, J.H. Byun, Tissue-engineered bone formation using periosteal-derived cells and polydioxanone/pluronic F127 scaffold with pre-seeded adipose tissue-derived CD146 positive endothelial-like cells, Biomaterials 32 (22) (2011) 5033–5045.

[17] P. Zamiri, Y. Kuang, U. Sharma, T.F. Ng, R.H. Busold, A.P. Rago, L.A. Core, M. Palasis, The biocompatibility of rapidly degrading polymeric stents in porcine carotid arteries, Biomaterials 31 (31) (2010) 7847–7855.

[18] Y. Li, Y. Xie, B. Li, Z. Xie, J. Shen, S. Wang, Z. Zhang, Initial clinical experience with the biodegradable absnow(TM) device for percutaneous closure of atrial septal defect: a 3-year follow-up, J. Intervent. Cardiol. 2021 (2021), 6369493.

[19] M.J. Mullen, D. Hildick-Smith, J.V. De Giovanni, C. Duke, W.S. Hillis, W. L. Morrison, C. Jux, BioSTAR Evaluation STudy (BEST): a prospective, multicenter, phase I clinical trial to evaluate the feasibility, efficacy, and safety of the BioSTAR bioabsorbable septal repair implant for the closure of atrial-level shunts, Circulation 114 (18) (2006) 1962–1967.

[20] B. Li, Z. Xie, Q. Wang, X. Chen, Q. Liu, W. Wang, Y. Shen, J. Liu, A. Li, Y. Li, G. Zhang, J. Liu, D. Zhang, C. Liu, S. Wang, Y. Xie, Z. Zhang, J. Ding, Biodegradable polymeric occluder for closure of atrial septal defect with interventional treatment of cardiovascular disease, Biomaterials 274 (2021), 120851.

[21] C. Jux, H. Bertram, P. Wohlsein, M. Bruegmann, T. Paul, Interventional atrial septal defect closure using a totally bioresorbable occluder matrix: development and preclinical evaluation of the BioSTAR device, J. Am. Coll. Cardiol. 48 (1) (2006) 161–169.

[22] W.B. Ou-Yang, S.Z. Wang, S.S. Hu, F.W. Zhang, D.W. Zhang, Y. Liu, H. Meng, K. J. Pang, L.K. Meng, X.B. Pan, Perventricular device closure of perimembranous ventricular septal defect: effectiveness of symmetric and asymmetric occluders, Eur. J. Cardio. Thorac. Surg. 51 (3) (2017) 478–482.

[23] K. Ishikiriyama, M. Pyda, G. Zhang, T. Forschner, J. Grebowicz, B. Wunderlich, Heat capacity of poly-p-dioxanone, J. Macromol. Sci., Part B 37 (1) (1998) 27–44.

[24] Z.X. Zhou, X.L. Wang, Y.Z. Wang, K.K. Yang, S.C. Chen, G. Wu, J. Li, Thermal properties and non-isothermal crystallization behavior of biodegradable poly (p-dioxanone)/poly (vinyl alcohol) blends, Polym. Int. 55 (4) (2006) 383–390.

[25] A. Dumitrescu, G.K. Lane, J.L. Wilkinson, T. Goh, D.J. Penny, A.M. Davis, Transcatheter closure of perimembranous ventricular septal defect, Heart 93 (7) (2007), 867-867.

[26] N.J. Collins, L. Benson, E.M. Horlick, Late complete heart block in an adult patient undergoing percutaneous ventricular septal defect closure, J. Invasive Cardiol. 20 (6) (2008).

[27] D. Pavcnik, K. Takulve, B.T. Uchida, M. Pavcnik Arnol, W. VanAlstine, F. Keller, J. Rösch, Biodisk: a new device for closure of patent foramen ovale: a feasibility study in swine, Cathet. Cardiovasc. Interv. 75 (6) (2010) 861–867.

[28] M. Sigler, B. Söderberg, B. Schmitt, A. Mellmann, J. Bernhard, Carag bioresorbable septal occluder (CBSO): histopathology of experimental implants, EuroIntervention 13 (14) (2018) 1655–1661.

[29] S. Toumanides, E.B. Sideris, T. Agricola, S. Moulopoulos, Transcatheter patch occlusion of the left atrial appendage using surgical adhesives in high-risk patients with atrial fibrillation, J. Am. Coll. Cardiol. 58 (21) (2011) 2236–2240.

[30] W.C. Yip, F. Zimmerman, Z.M. Hijazi, Heart block and empirical therapy after transcatheter closure of perimembranous ventricular septal defect, Cathet. Cardiovasc. Interv. 66 (3) (2005) 436–441.

[31] Y. Shen, W. Zhang, Y. Xie, A. Li, X. Wang, X. Chen, Q. Liu, Q. Wang, G. Zhang, Q. Liu, J. Liu, D. Zhang, Z. Zhang, J. Ding, Surface modification to enhance cell migration on biomaterials and its combination with 3D structural design of occluders to improve interventional treatment of heart diseases, Biomaterials 279 (2021), 121208.

[32] I. Martinez de Arenaza, N. Hernandez-Montero, E. Meaurio, J.-R. Sarasua, Competing specific interactions investigated by molecular dynamics: analysis of poly (p-dioxanone)/poly (vinylphenol) blends, J. Phys. Chem. B 117 (2) (2013) 719–724.

[33] M. Pan, Z. Xu, W. Luo, Y. Yang, T. Teng, J. Lin, H. Huang, In vitro and in vivo properties study of a novel 3D-printed absorbable pancreaticojejunostomy device made by melting blended poly (p-dioxanone)/poly (lactic acid), Mater. Des. 210 (2021), 110088.